NASA/TP-1998-208429

Quantitative Examination of Corrosion Damage by Means of Thermal Response Measurements

Nik Rajic
Langley Research Center, Hampton, Virginia

National Aeronautics and
Space Administration

Langley Research Center
Hampton, Virginia 23681-2199

June 1998

Available from the following:

Quantitative Examination of Corrosion Damage By Means of Thermal Response Measurements

Nik Rajic

Abstract

Two computational methods are presented that enable a characterisation of corrosion damage to be performed from thermal response measurements derived from a standard flash thermographic inspection. The first is based upon a one dimensional analytical solution to the heat diffusion equation and presumes the lateral extent of damage is large compared to the residual structural thickness, such that lateral heat diffusion effects can be considered insignificant. The second proposed method, based on a finite element optimisation scheme, addresses the more general case where these conditions are not met. Results from an experimental application are given to illustrate the precision, robustness and practical efficacy of both methods.

1 Introduction

Infrared thermography is widely acclaimed as offering a uniquely practical means of non-destructive inspection, yet is also often maligned because the data it produces is not readily interpretable in a quantitative sense. Two fundamental problems have traditionally hindered attempts at flaw characterisation: heat conduction and the particularly poor intrinsic signal-to-noise levels of photon-detection devices. Fortunately, both have been substantially mitigated by recent technological advancements. Improved infrared detection equipment along with powerful image processing hardware have led respectively to better data quality and to the facilitation of various computational means of addressing the heat conduction problem.

These developments have had an important bearing on the problem of hidden corrosion damage in aging aircraft, an issue that leapt to prominence after the identification of corrosion as a contributing factor in the 1988 Aloha Airlines B737 accident. Since then, significant efforts have been made toward developing effective means of estimating the severity of corrosion damage on the basis of data acquired from a thermographic inspection. Existing strategies fall roughly into one of two categories: those that address the core inverse thermal problem by a rigorous analytical approach, and those that combine empiricism with elements of mathematical modelling. Both have specific advantages but neither appears to have spawned an entirely satisfactory general solution that is precise and robust, yet practical enough for routine field implementation. Some of these studies do however afford a valuable insight into the aspects of the problem that are keys to its resolution in these terms. The intention of the present article is to report on two strategies that focus on some of these key aspects. The section that follows describes in general terms the relevant inverse problem to be solved and presents an overview of the literature addressing its solution.

1.1 The Inverse Thermal Problem - An Overview

The structural characterisation of a corroded component based on its thermal response to an external thermal stimulation involves an inverse thermal problem; sometimes called the "unknown boundary" inverse problem. Its basic statement is thus: to determine the profile or a particular characteristic of an inaccessible surface given measurements of the thermal response to a thermal excitation applied upon a different surface. When posed in a sufficiently idealised form, problems like these can be solved in a reasonably rigorous analytical manner.

Hseih & Kassab (1986) present a strategy tailored for the two-dimensional boundary identification problem involving steady state thermal conditions. A rigorous solution was made possible by a coordinate mapping scheme that successfully transformed the original specimen geometry with its unknown rear boundary profile, to a regular rectangular domain. In this form, the problem has a steady state solution that can be expressed in terms of a single fourier series whose coefficients are uniquely determined by the steady temperatures measured on the surface to which the excitation is applied. After these coefficients were found, and the temperature distribution throughout the auxilliary domain constructed from them, the profile of the hidden surface was found simply as the locus within the domain along which boundary conditions, assumed or known to apply on this surface, were satisfied. Whilst the method was shown to perform well with numerically generated data and was robust when applied to data containing low levels of simulated noise, its reliance on steady state conditions is clearly inconsistent with current implementations of flash thermography. Banks et al (1989) present a more useful though far more complex analytical development based upon the method of mappings to solve the same type of two-dimensional problem but without the steady-state constraint. The method was applied to several idealised corrosion problems with good success and despite the generally ill-conditioned nature of such inverse problems, with reasonable robustness.

Inverse thermal problems can alternatively be tackled using a wave formalism (Green (1927)), in which heat diffusion is mathematically treated as a wave propagation phenomenon (see for example Pade & Mandelis (1993)). A notable advantage it offers is the accompanying large body of knowledge pertaining to the solution of analogous inverse problems in x-ray and acoustic diffraction. Crowther et al (1993) report on the application of a wave-like treatment to a three-dimensional inverse problem involving the estimation of the lateral shape of a semi-infinite void contained within a half plane at a known depth. The forward problem was cast in terms of a convolution between a Green's function embodying a description of thermal wave scattering processes, and a defect shape function representing the scattering object. The corresponding inverse problem was solved by standard frequency domain deconvolution techniques. Results obtained on flash-heated steel plate specimens containing planar defects of irregular shape confirmed that the method could provide both good shape reconstruction and seemingly good robustness. Unfortunately, the method presumes an apriori knowledge of the flaw depth, a parameter that is normally assumed to be an unknown. The theory was later extended to include non-planar defects and anisotropic material properties (Favro et al (1994)), though its presumption of a known defect depth remained.

Many problems arise in practice that are simply not amenable to a rigorous analytical approach. From the outset, a problem may be impossible to structure in a mathematically tractable form, perhaps because of a complex geometry, or, when a solution is possible, it may lack sufficient robustness. In these situations, an empirical approach or one combined with rudimentary modelling may offer the only means of obtaining a useful solution. An especially simple treatment was presented by Del Grande et al (1993). Here, it was shown to be possible to linearly relate the temperature rise measured on a structure at a specific point and at a fixed time after flash excitation, to the amount of material loss at that point. Whilst effective, such an approach has the serious disadvantage of requiring renewed calibration for even slight variations in the experimental configuration. The need for extensive calibration can often be avoided by way of a simple mathematical model. A case in point is the method presented by Vavilov et al (1996). Here, standard one-dimensional heat diffusion theory was applied to produce a simple rational expression of the form,

$$\frac{\Delta L}{L_{ref}} = \frac{\frac{\Delta T}{T_{ref}}}{1 + \frac{\Delta T}{T_{ref}}}$$

where ΔT is the temperature difference between the point of observation and a reference point located within a defect-free region (T_{ref}), and ΔL and L are the corresponding thickness measurements. Application of the expression was restricted to within what the authors describe as an "optimal observation time", defining a period during which lateral diffusion effects; not encompassed by the 1-D formulation; are insignificant. Experimental results were most encouraging for only relatively shallow flaws. Other semi-empirical methods may be found in the review by Maldague (1993).
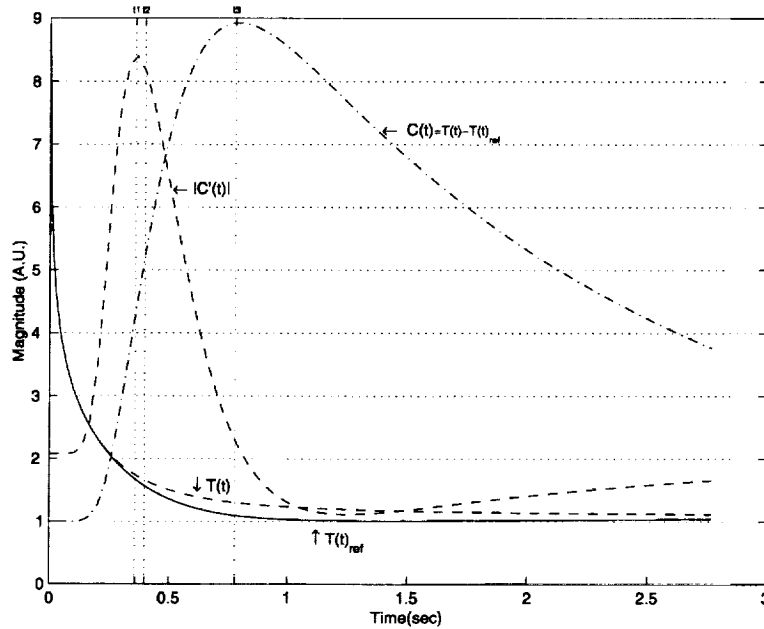

Figure 1: Sample of a typical evolution of contrast C as a function of time following the impulse excitation of a structure containing a flaw. T is the temperature above the flaw, T_{ref} is the temperature at a reference location and the characteristic times t_1, t_2, and t_3 respectively refer to the time to contrast inflection, the time to $\frac{1}{2}$ peak contrast and the time to peak contrast.

Any approach reliant upon measurements of temperature magnitude stands to be biassed by the various parasitic influences that tend to accompany these measurements. Relevant effects include: non-uniform illumination, extraneous reflections, non-uniform infrared emissivity and to a lesser extent those effects related to the imager itself, like detector gain non-uniformity and optical distortion caused by lens abberations. If not accounted for, these can lead to spurious flaw detections and can hinder attempts at characterising an existing flaw. An increasingly popular alternative is to examine the temporal characteristics rather than the absolute values of the temperature response, since these tend not to be influenced nearly as much by the forenamed effects. The evolution of contrast; that is the temperature difference between a point of interest and a reference point known to reside in a sound area; contains several distinct epochs that are strong functions of the characteristics of an underlying flaw (Fig 1). Some of these have especially useful properties. The time to contrast inflection for instance has been shown by Favro (1995) as well as being pointed out by others, to be especially well suited to the characterisation of flaw depth, based largely on its relative insensitivity to the lateral extent of a flaw. The independence stems directly from its manifestation during the very early parts of the contrast evolution, during a period when lateral (in-plane) heat diffusion is insignificant as compared to through-thickness diffusion. The point is significant because it suggests that in

order to facilitate a simple approach to a characterisation problem it is fundamentally important to restrict the analysis to a time frame where diffusion is largely confined to one spatial dimension; in the through-thickness direction. This key principle underlies an approach presented in the following section that tackles the corrosion characterisation problem. To illustrate some of its inherent advantages we apply the method to numerically generated data pertaining to a simulated two-dimensional corrosion problem, and then to experimental data involving several two-dimensional specimens containing simulated corrosion damage.

2 A One-Dimensional Approach

The approach is described as follows. Consider a two dimensional structure containing a simple rectangular 'cutout' flaw. An approximate representation of this body is constructed by assuming it to be comprised of two thermally isolated slabs of different thickness (Fig 2).
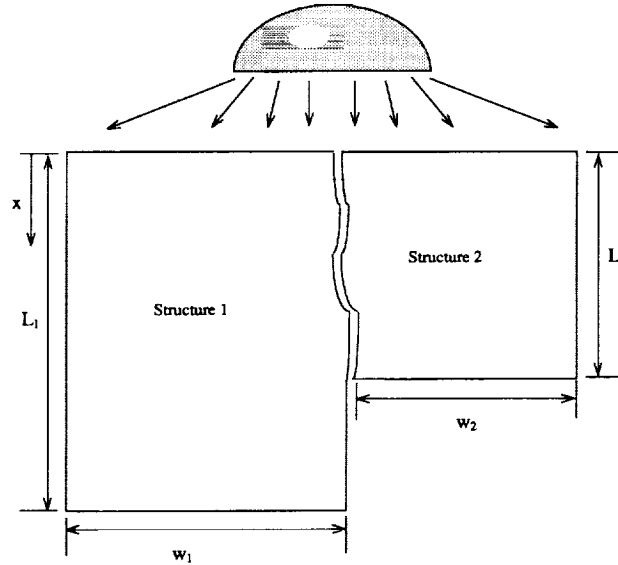

Figure 2: Two-dimensional structure containing a rectangular flaw. Depicted in a one-dimensional approximation as two independent bodies of different thickness.

A plane impulse heat source of intensity Q applied to the surface of the slab of thickness L_1 produces the following temperature response at the surface $x = 0$, (Carslaw & Jaeger (1959)),

$$T_1(t) = \frac{Q\alpha}{KL_1} \left(2\sum_{k=1}^{\infty} e^{-\alpha\left(\frac{k\pi}{L_1}\right)^2 t} + 1 \right). \tag{1}$$

Here, α is the thermal diffusivity and K is the thermal conductivity. The temperature difference that would exist between this and a thinner structure, say of thickness L_2, exposed to the same excitation, follows from Eq. (1),

$$C(t) = T_2(t) - T_1(t) = \frac{2Q\alpha}{K} \left[\sum_{k=1}^{\infty} \left(\frac{1}{L_2} e^{-\frac{k^2\beta t}{L_2^2}} - \frac{1}{L_1} e^{-\frac{k^2\beta t}{L_1^2}} \right) + \frac{L_1 - L_2}{2L_2 L_1} \right], \qquad L_1 > L_2 \tag{2}$$

where

4

$$\beta = \alpha \pi^2$$

and $C(t)$ we refer to as the contrast. Consider now the evolution of contrast predicted by Eq. (2) for the following three different specimen configurations: values of α, K, and L_1 are fixed at 60 mm^{2}sec^{-1}, 154 Wm^{-1}K^{-1}, and 10 mm respectively and the thickness L_2 is varied amongst three values; 2 mm, 3 mm and 5 mm. The corresponding solutions for $C(t)$ are presented in Fig 3 and are denoted by unmarked lines. The additional set of curves, denoted by marked lines, represent solutions to the two-dimensional problem created by joining the two slabs together where the widths defined in Fig 2 were chosen as $w_1 = 25$ mm and $w_2 = 5$ mm. This problem was solved using the finite element method with a mesh comprised of linear rectangular elements, 10 in depth and 24 in width, and with adiabatic conditions assumed on all boundaries. The contrast here is a function of lateral position but for illustrative purposes we consider only the contrast at the extreme right hand side of the structure, defined in reference to the response at the extreme left. The feature to note in the figure is the close accordance between the related one and two-dimensional solutions in the early stages of the contrast evolution, say for the period extending from the onset of the excitation until 1/10th of a second after its termination. This clearly implies that, within such a period of time, lateral heat diffusion effects are unimportant in describing the surface temperature response. By ignoring these effects the inverse problem needed to be solved in order to determine the amount of material loss is greatly simplified — in essence only the thickness of the shorter slab in the one-dimensional representation is to be found.
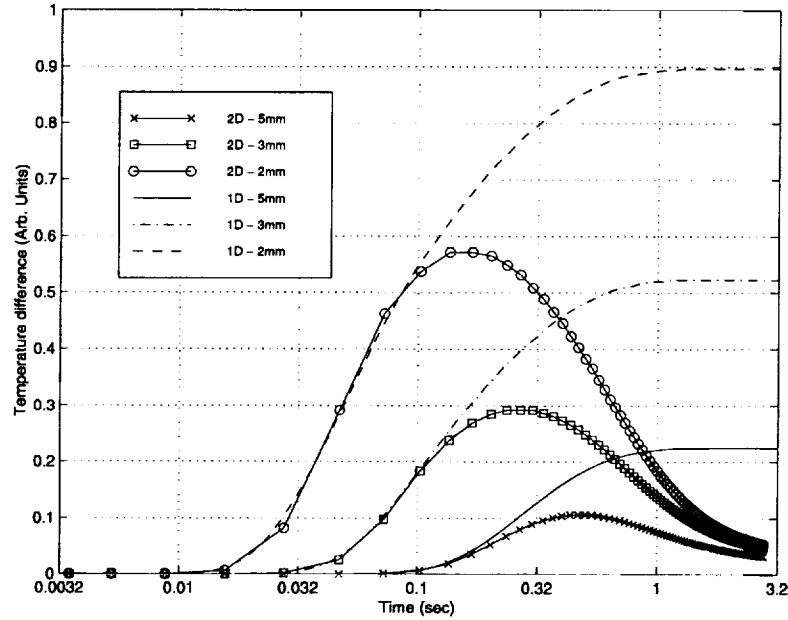

Figure 3: Contrast evolutions for 1-D (analytical) and 2-D (Finite element) treatments for various values of L_2

A direct solution for the thickness L_2 in Eq. (2) is sought, making only the assumptions that the reference thickness L_1, and the material properties α and K, are known. After rearranging the original expression, Eq. (2), an objective function is constructed in terms of two unknowns as follows

$$\chi = \sum_{j=1}^{N} \left[\theta_j - A \left(\frac{1}{L} \sum_{k=1}^{M} (\frac{1}{\gamma} e^{\frac{-\beta k^2 t_i}{\gamma^2}} - e^{-\beta k^2 t_i}) + \frac{1-\gamma}{2\gamma L} \right) \right]^2, \tag{3}$$

5

where N is the number of data points, M is the number of eigenvalues, θ is the measured contrast and the parameters to be estimated are the thickness ratio $\gamma = L_2/L_1$, and a scaling parameter A. Note that from hereon the subscript on L_1 is dropped with the understanding that L refers to the reference thickness. The scaling parameter is required to account for the fact that in practice only a poor knowledge of the excitation intensity is expected and more often than not the data obtained is likely to be uncalibrated. The only assumptions are that the experimental contrast-data has zero offset, that is $C_{t\to 0} \to 0$, and that the data is normalised so that the peak value is scaled to L^{-1}. Such normalisation has little direct bearing on the solution process itself, however it does facilitate a measure of the 'one-dimensionality' of the experimental data, since in a purely one-dimensional case the scale parameter may then be related to the thickness ratio as follows: $A = 2\gamma/(1 - \gamma)$.

The minimisation of χ is not amenable to a closed form solution, but it can be done efficiently with standard numerical optimisation techniques. The objective function surface takes the characteristic form presented in Fig 4. Note that since the inverse of χ is shown here, the solution corresponds to a maximum rather than a minimum value. The asymptotic behaviour of the function can be defined as follows: for variations in γ we have $\chi \to \sum \theta^2$ as $\gamma \to 1$ and $\chi \to \infty$ as $\gamma \to 0$ and for variations in A we have $\chi \to \sum \theta^2$ as $A \to 0$ and $\chi \to \infty$ as $A \to \infty$. The solution is found along a narrow ridge (or valley) that extends in the direction of near constant γ at a value close to the optimal solution. Data used in constructing the function were obtained from a finite element solution of the two-dimensional cutout problem described earlier. For this case, the thickness ratio of 0.5 used in the simulation accords well with the optimal value of near $\gamma = 0.5$ indicated by the projected contour. Note that the apparent local maxima near the global maximum are an artefact of the low sampling resolution used in plotting the function. The solution is in fact unique.
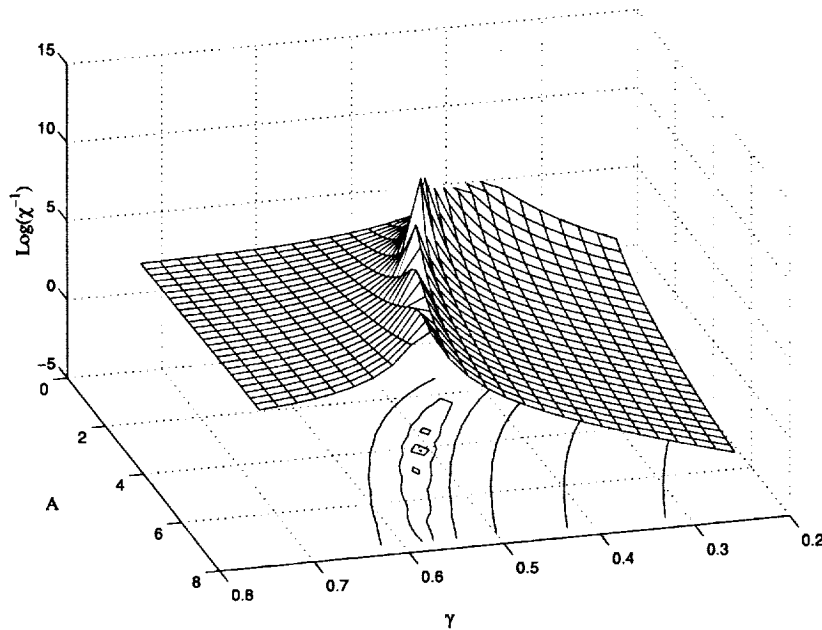

Figure 4: Surface of χ^{-1}.

Given the well behaved nature of the objective function almost any optimisation scheme should suffice in solving the problem irrespective of the quality of the initial estimates. The only remaining important issue is that of computational efficiency. For such functions, gradient based methods typically outperform methods based solely on the evaluation of the function itself. For the problem at hand, both conjugate gradient and quasi-newton methods were found to be clearly superior to the simplex method. The partial derivatives of the objective function are trivially evaluated, viz.,

$$\frac{\partial \chi}{\partial A} = \sum_{j=1}^{N} 2\phi_j \left(\frac{1}{L} \sum_{k=1}^{M} (\frac{1}{\gamma} e^{\frac{-\beta k^2 t_i}{\gamma^2}} + e^{-\beta k^2 t_i}) + \frac{1-\gamma}{2\gamma L} \right),$$

$$\frac{\partial \chi}{\partial \gamma} = \sum_{j=1}^{N} 2\phi_j \left(\frac{1}{L} \sum_{k=1}^{M} \frac{1}{\gamma^4} e^{\frac{-\beta k^2 t_i}{\gamma^2}} \left(2\beta k^2 t_i - \gamma \right) - \frac{1}{2\gamma^2 L} \right), \tag{4}$$

where,

$$\phi_j = \theta_j - A \left(\frac{1}{L} \sum_{k=1}^{M} (\frac{1}{\gamma} e^{\frac{-\beta k^2 t_i}{\gamma^2}} + e^{-\beta k^2 t_i}) + \frac{1-\gamma}{2\gamma L} \right).$$

All subsequent optimisations of Eqn (3) presented in this study were obtained using the conjugate gradient technique.

2.1 Numerical Validation

Issues of precision and robustness were examined by applying the model to a test case created by finite element simulation. It involved a two dimensional 60 mm x 10 mm rectangular aluminium specimen with a section 2 mm deep and 10 mm wide removed from the back surface so as to simulate material loss due to corrosion. The structure was modelled using a 24 × 10 linear rectangular element discretisation scheme (Fig 5) and the excitation (applied at $y = 0$) consisted of a fixed intensity pulse of 20 ms duration. After solving the heat conduction problem, the contrast at each surface nodal point was determined in reference to the response at the extreme left or right hand surface nodal points (equivalent by symmetry), and then sampled at a rate of 30 Hz so as to mimic acquisition in the RS170 video signal format. As a result of the low sampling rate, only the first 15 data points in the contrast evolution at each surface nodal could be used in the optimisation process. The first objective of the validation was to estimate the depth ratio γ at each surface nodal point so as to examine how well the model could predict the flaw depth and the back surface profile in general.

Estimates for γ and A determined from the contrast evolutions are plotted as a function of surface position in Fig 6, whilst the values of γ, scaled to length, are superimposed on the mesh in Fig 5. The estimated distribution of γ as a function of lateral position has a Gaussian shape. At the cutout, the discrepancy in predicted depth ranges from a peak of 5% at the mid-point to practically nil at the edges. Some error is always to be expected since the one-dimensional model can never provide a complete description of what is clearly a two-dimensional heat conduction process. Stated simply, since diffusion implies an instantaneous transfer of information, two-dimensional effects are manifest in the surface response at the moment the excitation is applied. The key point however is that the discrepancies caused by this will tend to be small, as seen in the current example, when only the early stage of the contrast evolution is considered. Where larger errors are expected is in the sound region adjacent to the flaw. Here, the contrast evolution is solely an artefact of lateral heat conduction effects and so it comes as no surprise that the model fails to track precisely the abrupt change in back surface shape. Nonetheless, one obtains quite a useful shape prediction that would probably suffice for most practical purposes. A notable feature in Fig. 6 is the abrupt change in the spatial gradient of A near the flaw edge. This is symptomatic of the effects of lateral heat diffusion and could thus potentially yield a useful measure of the efficacy of the corresponding γ estimates.
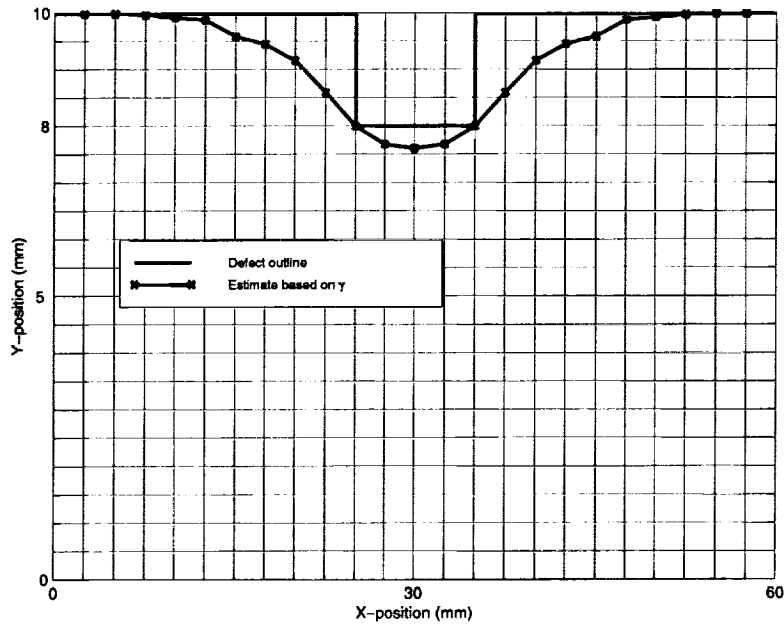
Figure 5: 24 × 20 rectangular element discretisation of the 60 × 10 mm specimen domain. Shown also is the flaw outline and the outline constructed from values of γ estimated from the contrast response at each surface nodal point.
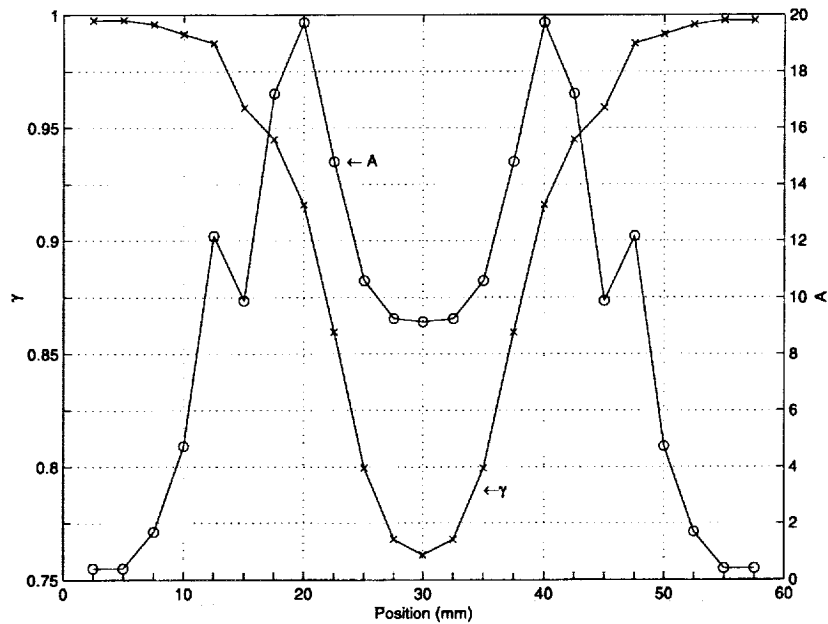

Figure 6: Plot of γ and A for the simulated case as a function of position across the specimen. The flaw spans the range 25 – 35 mm.

8

2.1.1 Robustness

The model was next applied to simulated data corrupted with known levels of numerically generated normally-distributed noise. Presented in Table 1 are the relevant statistics for the (γ, A) estimates obtained from data taken at the central node. Listed values, with the exception of those pertaining to the noise free case, represent an average of twenty individual results. Two noise levels were considered, each characterized by a signal to noise ratio calculated from power spectral decompositions of the contrast and noise signals.

Table 1: Arithmetic mean (μ) and standard deviation (σ) of estimates obtained from noisy data.

	μ_{SNR}	$\mu\gamma$	$\sigma\gamma$	μ_A	σ_A
No noise	∞	0.76	0	9.3	0
Noise - case 1	4.16	0.73	0.08	14.02	10.57
Noise - case 2	0.38	0.73	0.19	16.07	13.82

The addition of noise is seen to cause only a slight bias in the mean value of γ; the 4 % discrepancy is more than acceptable in view of the sparseness of the contrast evolution data (comprising only 15 points, as stated earlier). The standard deviations in both γ and A indicate good robustness, a feature that is perhaps better illustrated with the help of the graph in Fig 7. Here, an indication is given that high levels of noise have little impact on the thickness estimate as long as the shape of the contrast evolution is preserved. Clearly, a large data population and a high SNR are advantageous. As a final comment, it is worth pointing out that methods based on a single characteristic time, the time to contrast inflection for instance, are not expected to perform anywhere near as well under the noise conditions considered here.
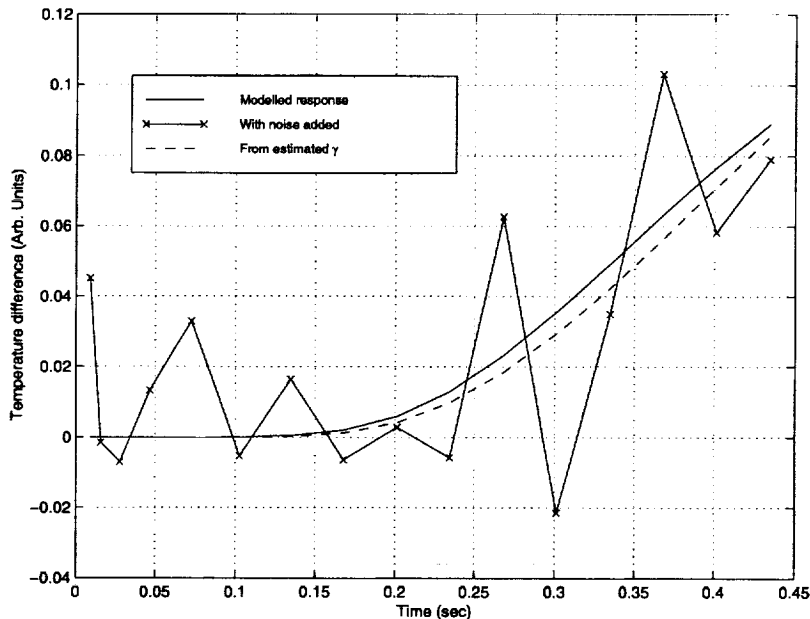

Figure 7: Contrast response with noise added (SNR=0.61) as well as the response predicted from estimated values of γ (= 0.81) and A (= 19.55).

9

2.2 Experiment Results and Discussion

Because of limitations in the performance capabilities of the available thermal imaging equipment, the experimental investigation had to be focused on specimens with rather severe levels of simulated corrosion damage (Fig 8). The indicated specimens were manufactured from an Al2024 alloy with the following assumed thermal properties: $\alpha = 49$ mm^2 sec^{-1}, and $K = 125$ Wm^{-1}K^{-1}. The thermal excitation source consisted of a 6 kJ photographic flash apparatus with a pulse duration presumed to be short enough to adequately approximate the impulse assumption used in the model formulation. Thermal response measurements were taken using an Inframetrics 760 scanning (HgCdTe) IR camera in RS170 analogue video signal format and then fed into a video image processor where the data was digitized to 8 bits and stored to disk. The n_t acquired frames were reduced to a single $n_x \times n_t$ array of pixel intensities I, where n_x is the number of pixels along the line AB (Fig 8). These data were found to contain a spatial trend which was evidently caused by the non-uniform application of illumination upon the specimen surface. The trend were removed by forming a quadratic function at each time interval j from a data set excluding the flawed region, i.e. $I_{i=1:10, n_x-10:n_x, j}$, and subtracting this from the complete set $I_{i=1:n_x, j}$. The contrast was then formed from the corrected data by subtracting the far field offset, O, as defined by the average pixel value about point A,

$$C_{i,j} = I_{i,j} - O_j, \tag{5}$$

where,

$$O_j = \frac{1}{n} \sum_{i=1}^{n} I_{i,j}.$$

Here, C is the contrast and $n = 5$ is a typical length for the averaging window. The optimisation, Eqn (3), was performed for each point i along the line AB with $\theta_j \equiv C_{i,j=1:N}$. Because of the slow sampling rate of the thermal imager (30 Hz), N tended to be small (less than 10 points).

The processed contrast evolution for the DFC specimen is shown in Fig 9 and the corresponding optimisation result is presented in Fig 10. The latter indicates a depth ratio of about 0.34 within the flawed region (between 25–35 mm), which corresponds quite closely to the known value of 0.4, only some 15 % in error. Note also that the variation about this average value is quite small. Moving away from the centre towards the flaw edge the change in γ across the edge into the unflawed region is not nearly as distinct as found in the simulation result (Fig 5), and indeed γ does not tend to the correct reference value of 1 at all, but maintains a steady value of near 0.3. This is thought to be at least partly attributable to the very low SNR away from the flawed region, though one cannot discount the possibility that the experimental data may have been biased by the residual effects of the non-uniform illumination mentioned earlier. By merely subtracting a quadratic offset one does not account for any induced lateral heat diffusion effects which could possibly bias the result. The importance of this result should not be overstated however since in practice it is almost always possible to reliably localise a defective region on the basis of the raw temperature image. The contrast response for the SFC specimen (Fig 11) was far cleaner than that for the DFC case and accordingly the estimates for the defect depth were noticeably better. Fig 12 shows both a more conclusive delineation between the defective and sound regions as well as a slightly better estimate for the defect depth, on average less than 10% in error. Remarkably, this result was achieved despite only 4 data points being used in the optimisation process. The tapered shape of the flaw is not well indicated in the estimates, as one should expect in view of the likely significance of lateral heat diffusion in these regions.

The proposed method has been shown to be capable of rendering useful estimates of flaw depth when the flaw extent is reasonably large in comparison to the residual specimen thickness. The method is not expected to perform equally well where this condition is not met, as may occur when the corrosion damage is highly localised. Under such circumstances, lateral heat diffusion effects cannot be considered insignificant
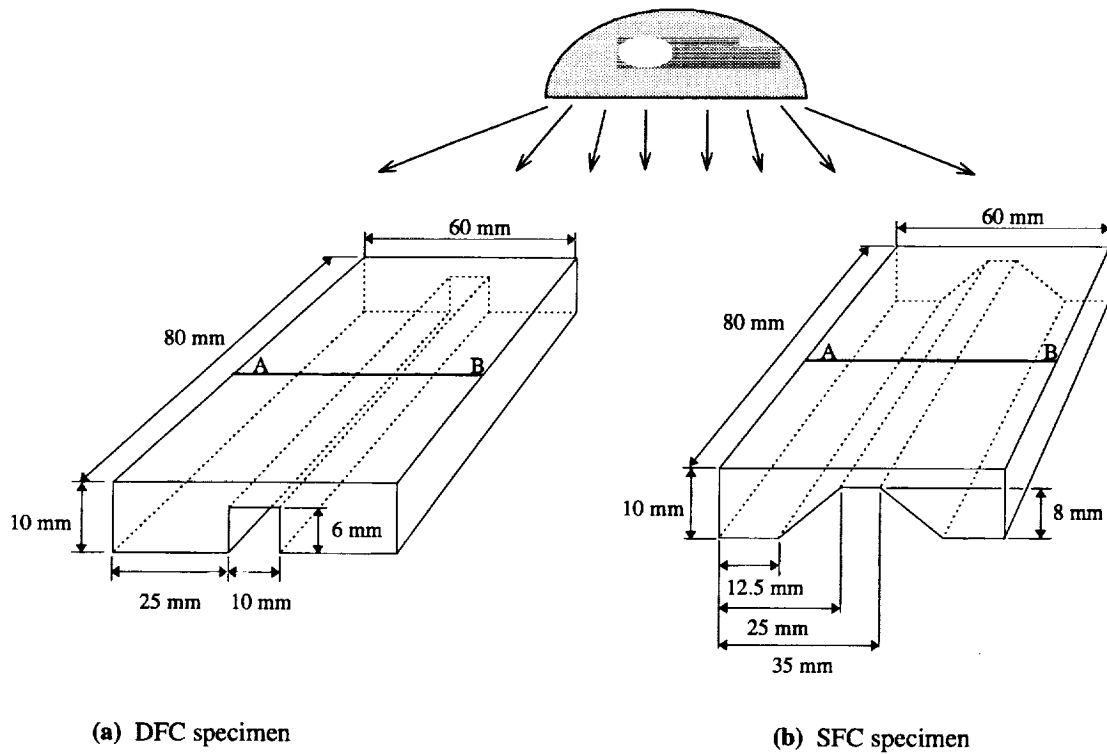
(a) DFC specimen **(b)** SFC specimen

Figure 8: Schematic showing both the deep flaw and the shallow flaw specimen configurations.
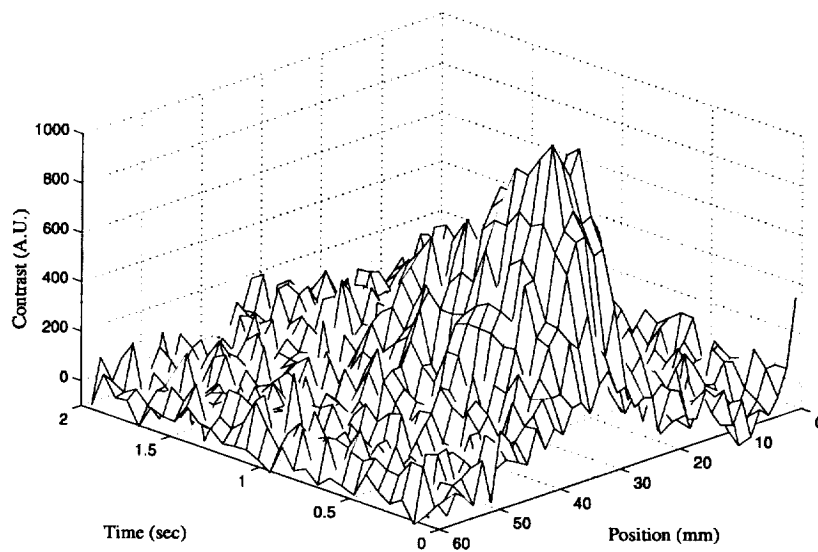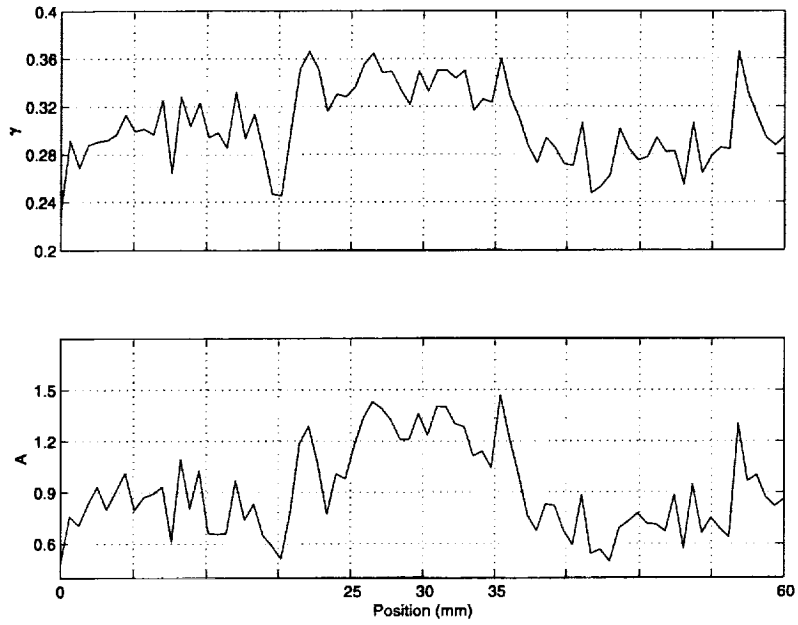

Figure 9: Contrast evolution for DFC specimen.

11

Figure 10: Results for DFC specimen ($\gamma = 0.4$). Optimisation performed at each spatial location using nine contrast-evolution data points.
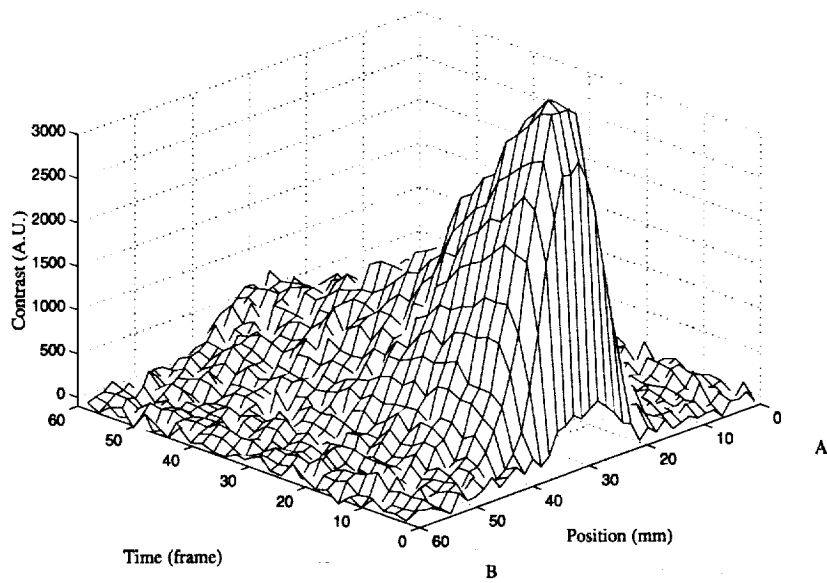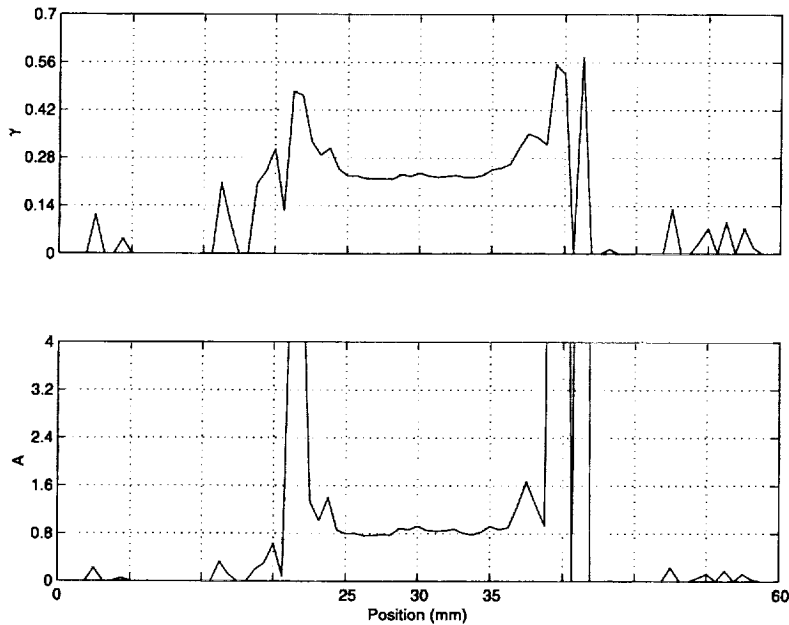

Figure 11: Contrast evolution for SFC specimen.

12

Figure 12: Results for DFC specimen (correct $\gamma = 0.2$). Optimisation performed at each spatial location using only four contrast-evolution data points.

and thus need to be taken into account in any attempt at solving the characterisation problem. Offered in the following section is an alternative strategy better able to handle such cases.

3   Finite Element Based Optimisation

As indicated in section 1.1, to include lateral heat diffusion effects in an analytical approach to the inverse problem would in most cases necessitate a drastic simplification of the actual problem, i.e. the half-plane assumption of Crowther et al (1993) and the steady state assumption of Hseih & Kassab (1986). Existing analytical studies do point to the fact however that these simplifications are necessary primarily in order to facilitate a solution to the relevant forward heat diffusion problem. This then raises the question of why not adapt a numerical technique to handle this forward component of the inverse problem; even profoundly complex forward heat conduction problems are solved trivially with numerical techniques like the finite element method.

Almost any inverse thermal problem should succumb to the following basic formula: first solve the forward problem for some arbitrary initial estimate for the defect shape. This shape is then modified by successive iterations of a non-linear optimisation scheme on the basis of the level of agreement between the temperature response as determined by the numerical solution and that measured experimentally. When no further improvement in the agreement can be achieved by modifying the current estimate for the flaw shape, that shape is assumed to be the solution. Two assumptions are fundamental and quite reasonable: (i) that a finite element model of the defect-free structure can be constructed and (ii) that the relevant thermal properties of the structure are known.

The computational efficiency of any such strategy is clearly an important consideration since the iterative application of a numerical means of solving a large heat conduction problem is likely to be computationally
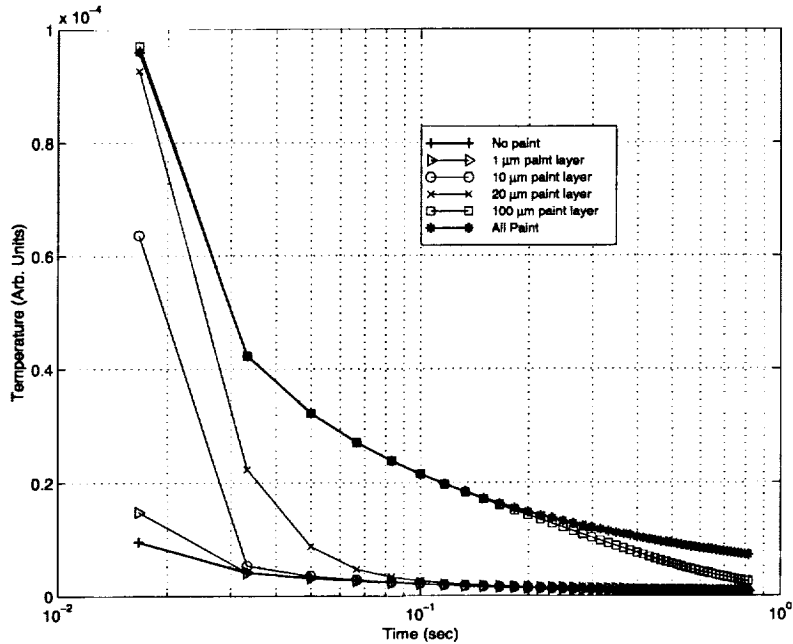
13

Figure 13: Surface temperature response as a function of time for a 10 mm thick aluminium plate with and without paint coating. To simulate data acquisition with a typical photon detector the response has been sampled at a 60 Hz rate and with an integration interval of 0.0167 second.

laborious. One of the most important ingredients for a quick solution is a carefully specified objective function. The obvious formulation would comprise the squared difference between the measured and calculated sets of primordial data.

$$\chi = \sum_{j=1}^{M} \sum_{i=1}^{N} (\theta_{i,j} - T_{i,j})^2, \tag{6}$$

where, respectively, θ and T are the measured and predicted temperature responses and i, and j represent spatial and time indices. Despite its simplicity and statistical efficiency, an objective function of this form is undesirable chiefly for the reason that absolute measurements are susceptible to the parasitic effects discussed earlier. Another important problem involves the layer of paint customarily applied to a target structure to enhance its infrared emmisivity. In comparison to the structure, this layer is usually extremely thin and so its impact on the measured temperature response is almost always considered negligible; that is, one normally assumes that the measurements are a function solely of the substrate. In reality however, this assertion rarely holds true in the early stages of the response if the excitation is short lived, as it invariably is when dealing with flash thermography. In fact, at the very onset of thermal excitation, the surface temperatures comprise almost entirely of the paint layer response. Figure 13 illustrates the effect of paint layer thickness on the measured response of an aluminium substrate as determined by an analysis presented in the Appendix. According to these results, even an unrealistically thin 1 μm coating of paint should have a measurable effect. Typical paint layer thicknesses exceed 20 μm. The implications of this are that if the primordial data are to be used, then the effect of any existing paint layer needs to be taken into account in the FE model.

The need for modelling the paint layer can be avoided by specifying an objective function in terms of elements of the temperature response that not only convey the characteristics important in defining the substrate structure but that are also independent of the paint layer properties. In doing this care needs

14

to be taken to include enough information to constrain the problem so that it yields an objective function topography with as few local minima as possible — ideally with a unique solution. An objective function was developed comprising of three terms that was shown after careful analysis to have these requisite properties. These components are as follows:

$$\chi_a = \frac{1}{M} \sum_{j=1}^{M} \sum_{i=1}^{N} \frac{(T_{i,j} - \bar{T}_j)(\theta_{i,j} - \bar{\theta}_j)}{\sqrt{(T_{i,j} - \bar{T}_j)^2 (\theta_{i,j} - \bar{\theta}_j)^2}}, \tag{7}$$

where $\bar{T}_i$, and $\bar{\theta}_i$ are the average values of the calculated and experimental temperatures respectively, and the subscripts i, and j are indices spanning N spatial and M time points respectively. The term represents the average correlation coefficient between the spatial shapes of the experimental and calculated data sets. The next term is

$$\chi_b = 1 - \frac{\sum_{i=1}^{N} \omega_i \frac{(t_i^{pc} - \tau_i^{pc})}{\max(t_i^{pc}, \tau_i^{pc})}}{\sum_{i=1}^{N} \omega_i}. \tag{8}$$

Here, t_i^{pc} represents the time taken for the calculated contrast evolution at point i to attain its maximum value, τ_i^{pc} is the corresponding time in the experimental data set, and ω_i represents a weighting factor applied to the time measurement at point i and is defined in relation to the absolute maximum contrast in the distribution, viz.,

$$\omega_i = \frac{C_i}{\max(C)}. \tag{9}$$

The final term is obtained by substituting the time to half peak contrast in place of the time to peak contrast in Eqn (3), viz.,

$$\chi_c = 1 - \frac{\sum_{i=1}^{N} \omega_i \frac{(t_i^{hpc} - \tau_i^{hpc})}{\max(t_i^{hpc}, \tau_i^{hpc})}}{\sum_{i=1}^{N} \omega_i}, \tag{10}$$

where hpc is an abbreviation for 'half peak contrast'. The complete objective function is formed by a weighted sum of all three terms as follows,

$$\chi = \frac{\lambda_a + \lambda_b + \lambda_c}{\lambda_a \chi_a + \lambda_b \chi_b + \lambda_c \chi_c}, \tag{11}$$

where λ_a, λ_b, and λ_c are weights for the components χ_a, χ_b, and χ_c respectively. Usually, one would weight all three components identically. A possible exception is where the time to half peak contrast occurs within the first few frames of data, as may occur with aluminium structures when sampling at conventional video rates. In this case the measure adds little information and should be weighted accordingly.

15

Constraining the defect shape to a distinct functional form greatly enhances the prospect of an efficient solution for the optimisation of χ. By its very nature, corrosion tends to produce damage of a characteristic shape that lends itself to a rather simple classification. The study is confined therefore to the four-parameter representation given in Fig 14, in which the hatched portion denotes a complete absence of material; corrosion products are not considered in the present study.
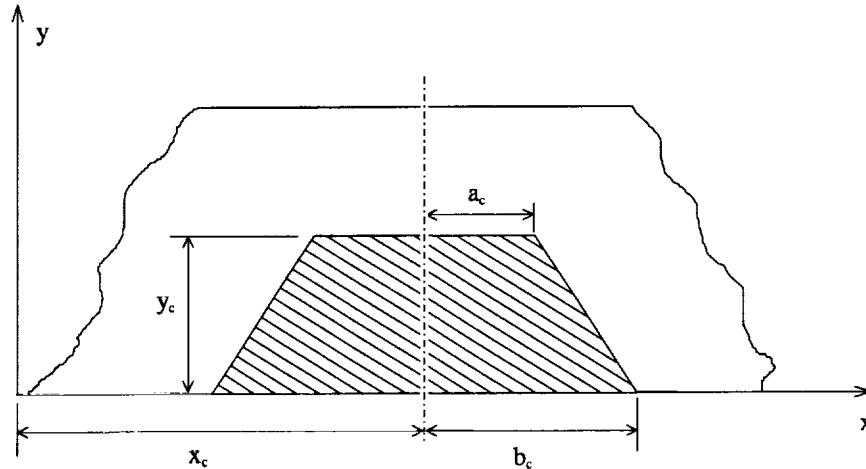

Figure 14: Schematic showing the 4 parameter functional description of corrosion damage used in solving the optimisation problem.

Obtaining an efficient solution to the forward heat diffusion problem is important as many such problems will need to be solved in the course of the optimisation process. Since most commercial finite element packages tend to have a large computational overhead, a dedicated finite element routine was written that was both computationally efficient and could be easily integrated with an optimisation routine. After assessing various optimisation strategies, an algorithm consisting of Powell's method with an enumerative discrete-step line searching strategy was settled upon. Communication between the optimisation and FEA programs consisted of only the values of the 4 parameters, x_c, y_c, a_c, b_c, and the objective function value χ.

The method was tested with numerically generated data and found to perform extremely well in terms of both precision and robustness. It was also found that convergence to a globally optimal solution in terms of the 4 parameters could be obtained most efficiently by performing an initial optimisation with the condition $b_c = a_c$. The solution to this smaller problem, dubbed the '3p' problem, was then used as an initial estimate for the full 4 parameter problem, dubbed the '4p' problem.

3.1 Experimental Results and Discussion

The method was applied to the experimental data described in section 2.2, for the aluminium SFC and DFC specimens (Fig 8). The results that follow may therefore be compared directly with those obtained by the one-dimensional method of the last section. A 24×10 element discretisation scheme was used throughout and solutions to the optimisation problem were obtained in all cases in under 1 minute of CPU time on a 200 MHz pentium processor. Figure 15 shows the value of χ as function of the number of the FE analyses performed, and Figs 16 and 17 show the shapes obtained upon completion of the optimisation process for the 3p and 4p cases respectively. The reconstruction shown in Fig 16 compares favourably to the known defect shape, with only a slight overestimation of both the vertical and horizontal size. A marginal improvement in both the level of fitness as defined by χ and the predicted shape, are seen in the 4p case (Fig 17).
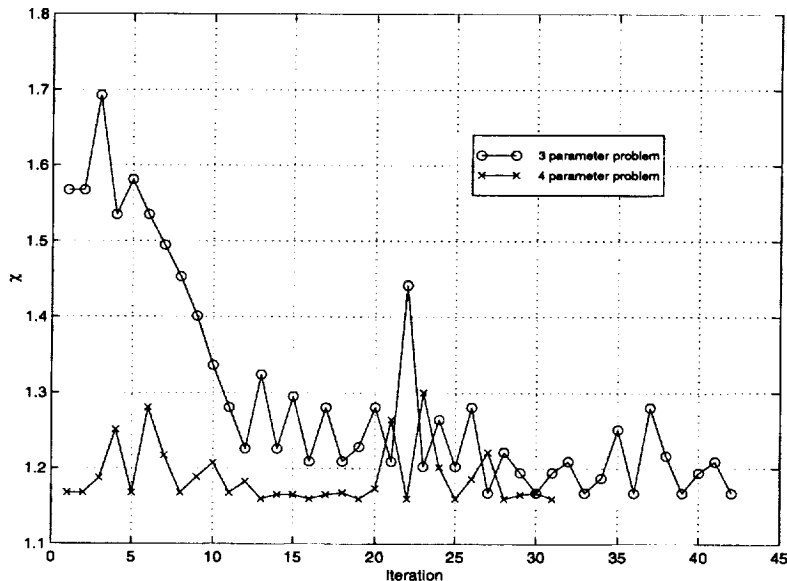
16

Figure 15: χ as a function of FEA iteration for DFC specimen.

A similar sequence of results are presented for the SFC specimen in Figs 18–20. Here the 4p solution (Fig 20) predicts the flaw depth well but not the irregular shape of the cutout. This is not surprising, and the reason why is perhaps best explained using the wave propagation paradigm. Assuming that the thermal excitation applied to the surface launches a series of thermal waves into the structure (Green (1927)), the contrast response can then be thought of as resulting from the reverbration of these waves. But in a diffusion process, any such waves are strongly attentuated with depth, much like electromagetic waves in a conducting solid are, so that the reflections emanating from deep within the specimen are necessarily much weaker than those from the shallower regions. As a consequence, the deeper structure of the flaw is only weakly represented in the measured contrast response. When combined with copious amounts of experimental noise and inconsistencies between the finite element model and experimental reality, the reconstruction of these deep features is seen to be an exceptionally challenging proposition.

The simplest way to improve these results overall is to improve the quality of the experimental data. This can be done in a number of ways, but perhaps most easily by simply modernising the thermal imaging equipment. The data used in the present work was acquired with an old system that has both a low sampling rate and poor intrinsic SNR compared to modern systems. Improvements could also be made by using higher intensity or multiple flash units and ensuring that the excitation is applied to the specimen as uniformly as possible so as to avoid inducing secondary lateral diffusion. Non-uniform illumination could alternatively be incorporated directly in the FE model, but this would require the additional effort of characterising the illumination distribution. No attempt was made in the present study to confirm the thermal properties given in section 2.2, though with no apparent systematic biases evident in the results, there appears to be little possibility of significant error.
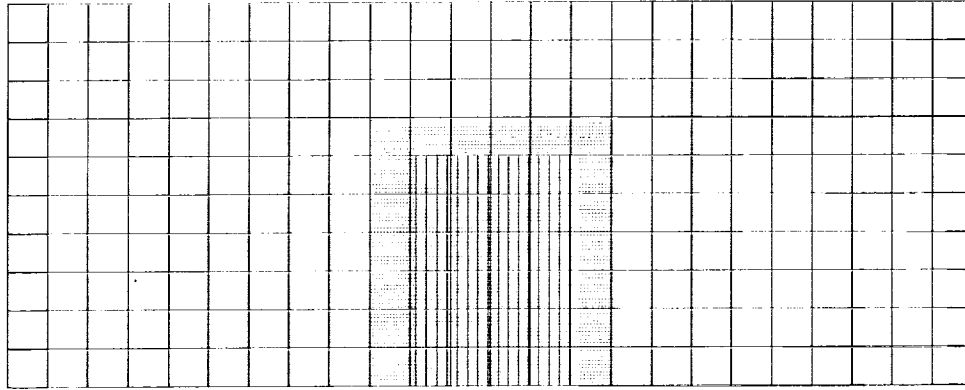
17

Figure 16: Optimal shape (horizontally hatched) compared to known flaw shape (vertically hatched) obtained from 3p solution for the DFC specimen data. Weightings were $\lambda_a = 1$, $\lambda_b = 1$, $\lambda_c = 0$.

4 Conclusion

Two independent methods have been presented that enable a characterisation of corrosion damage to be performed from thermal response measurements. Based upon a one dimensional analytical solution to the heat diffusion equation the first method was developed specifically for problems in which the lateral extent of damage is large compared to the residual structural thickness. Through both numerical and experimental applications the method was demonstrated to be robust enough to be applied to raw thermographic data and to yield depth estimates precise enough for most practical purposes. No prior calibration of the method is necessary and the only presumed knowledge is that of the specimen reference thickness and material thermal properties. Given its reliance on the early time history, the method is thought to be ideally suited to inspection systems with high frame-rate thermal imagers. Such systems should facilitate the application of the technique to thin-skinned structures on aircraft, a case that could not be considered with the equipment available in the present investigation.

The second method is based on a finite element optimisation scheme and can thus address problems where a one dimensional approach is not justified, such as where the residual specimen thickness and the lateral extent of the damage are of a similar scale. Experimental results indicated that despite its reliance on an iterative application of a finite element solution, the technique yields useful flaw characterisations within reasonable computational time. Although only two-dimensional problems were considered in the present study, the underlying principles are completely general. Indeed, a pseudo three-dimensional axisymmetric implementation is currently being applied to three-dimensional flaw structures. Work is also currently underway to assess the performance of both methods on specimens involving multilayered structures and corrosion byproducts. Results will be presented in a forthcoming report.
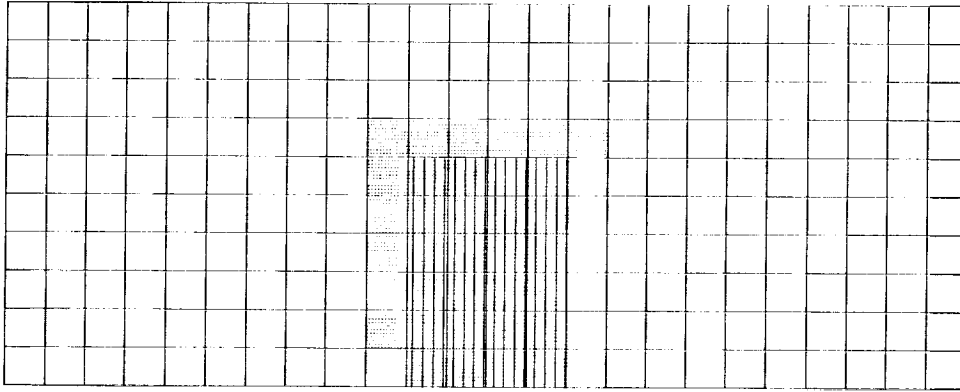
18

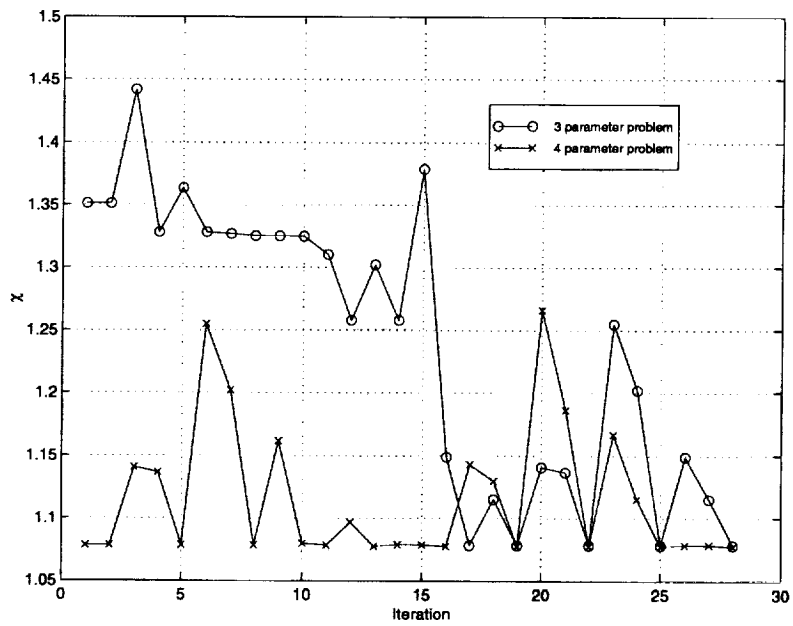Figure 17: As in the preceding figure except for 4 parameters.

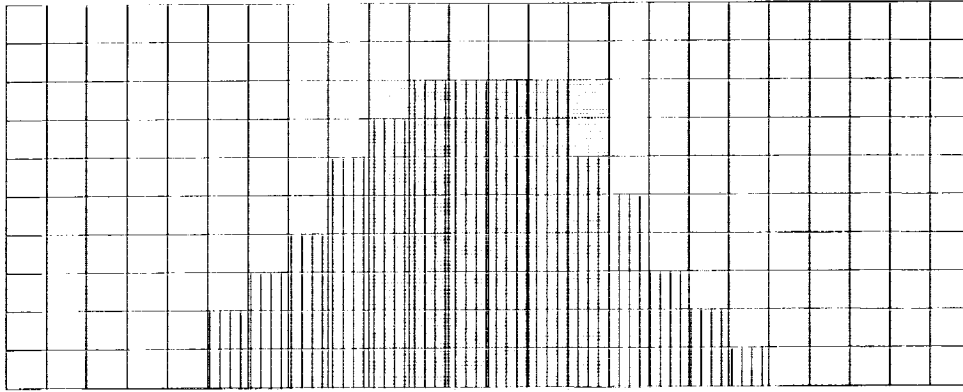Figure 18: χ as a function of FEA iteration for SFC specimen.

Figure 19: Optimal shape (horizontally hatched) compared to known flaw shape (vertically hatched) obtained from 3p solution for the SFC specimen data. Weightings were $\lambda_a = 1$, $\lambda_b = 1$, $\lambda_c = 0$.
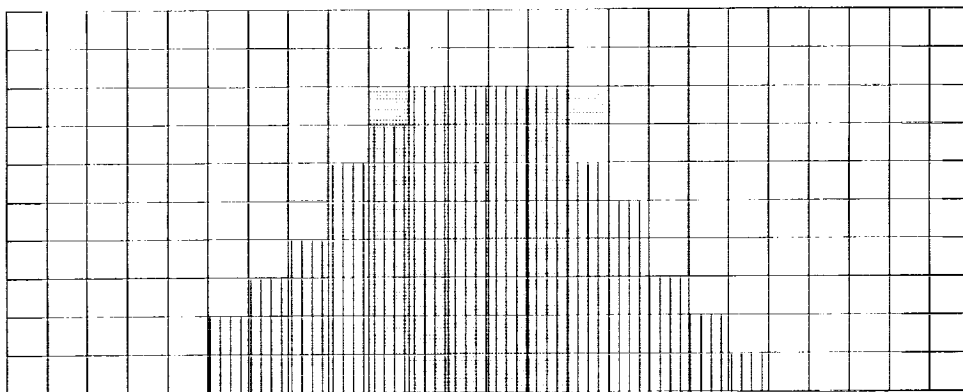

Figure 20: As in preceding figure except for 4 parameters.

5 Acknowledgments

6 References

Banks, H. T., Kojima, F., & Winfree, W. P.: Boundary Estimation Problems Arising in Thermal Tomography, *Inverse Problems,* Vol. 6, 1990, pp. 897–921.

Carslaw, H. S., & Jaeger, J. C.: *Conduction of Heat in Solids,* Second Ed., Oxford University Press (New York), 1959.

Crowther, D. J., Favro, L. D., Kuo, P. K., & Thomas, R. L.: Inverse Scattering Algorithm Applied to Infrared Thermal Wave Images, *J. Appl. Phys.,* Vol. 74, 1993, pp. 5828–5834.

Del Grande, N. K., Dolan, K. W., Durbin, P. F., Gorvad, M. R., & Shapiro, A. B.: *Dynamic Thermal Tomography for Nondestructive Inspection of Aging Aircraft,* Lawrence Livermore National Laboratory, UCRL-JC-112603, 1993.

Favro, L. D., Han, X., Kuo, P. K., & Thomas, R. L.: Improving the Resolution of Pulsed Thermal Wave Images with a Simple Inverse Scattering Technique, *Journal de Physique IV-C7,* 1994, pp. 545–551

Favro, L. D., Han, X., Kuo, P. K., & Thomas, R. L.: Imaging the Early Time Behaviour of Reflected Thermal-wave Pulses, SPIE–2473, 1995, pp. 162 –166.

Green, G.: Some Problems in the Conduction of Heat, *Phil. Mag.* S7, Vol. 3, 1927 pp.784–800.

Hseih, C. K., & Kassab, A. J.: A General Method for the Solution of Inverse Heat Conduction Problems with Partially Unknown System Geometries, *Int. J. Heat Mass Transfer,* Vol. 29, 1986, pp. 47–58.

Maldague, X. P. V.: *Nondestructive Evaluation of Materials by Infrared Thermography,* Springer Verlag (London.), 1993.

Özişik, N. K.: *Boundary Value Problems in Heat Conduction,* Dover (New York), 1989.

Pade, O., & Mandelis, A.: Computational Thermal-wave Slice Tomography with Backpropagation and Transmission Reconstructions, *Rev. Sci. Intrum.,* Vol. 64, 1993, pp. 3548–3562.

Tittle, C. W.: Boundary-Value Problems in Composite Media: Quasi-Orthogonal Functions, *Journal of Applied Physics,* Vol. 36, 1965, pp. 1486–1488.

Vavilov, V., Grinzato, E., Bison, P. G., Marinetti, S.: Surface Transient Temperature Inversion For Hidden Corrosion Characterisation: Theory and Applications, *Int. J. Heat Mass Transfer,* Vol. 39, 1996, pp. 355–371.

Appendix
Solution to the Two Layer Slab Problem

In this section we present a solution for the two-layer slab problem depicted in Fig 21 and then illustrate with a typical example the effect of paint layer thickness on the surface thermal response of a painted metal slab subject to a short-lived thermal excitation.
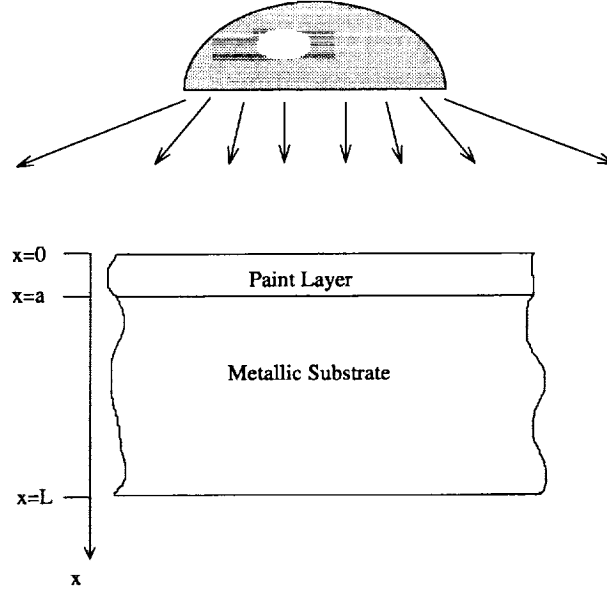

Figure 21: Painted structure subject to thermal excitation at surface $x = 0$.

An orthogonal-expansion approach is used to develop the solution (Tittle (1965) and Özişik (1989)). The temperatures in the two slabs satisfy the following equations,

$$\frac{\partial^2 T_1}{\partial x^2} + \frac{1}{k_1}\dot{Q}_1(x,t) = \frac{1}{\alpha_1}\frac{\partial T_1}{\partial t}, \qquad 0 < x < a, \tag{A1}$$

$$\frac{\partial^2 T_2}{\partial x^2} = \frac{1}{\alpha_2}\frac{\partial T_2}{\partial t}, \qquad a < x < L, \tag{A2}$$

subject to these boundary, interface and initial conditions,

$$\frac{\partial T_1}{\partial x} = 0 \quad \text{at} \quad x = 0, \tag{A3}$$

$$\frac{\partial T_2}{\partial x} = 0 \quad \text{at} \quad x = L, \tag{A4}$$

$$-k_1\frac{\partial T_1}{\partial x} = h(T_1 - T_2) \quad \text{at} \quad x = a, \tag{A5}$$

$$k_1\frac{\partial T_1}{\partial x} = k_2\frac{\partial T_2}{\partial x} \quad \text{at} \quad x = a, \tag{A6}$$

$$T_1(x,0) = 0; \quad T_2(x,0) = 0 \quad \text{at} \quad t = 0, \tag{A7}$$

22

where T is the temperature, k is the thermal conductivity, α is the thermal diffusivity, h is the interfacial thermal resistance, and the subscript $i = 1$ refers to the paint layer and $i = 2$ refers to the substrate. Note that heating of the paint surface is to be incorporated in the heat source term of Eq. (A1). A transient solution is sought using separation of variables, viz.,

$$T_i(x,t) = \sum_{n=1}^{\infty} \Phi_{in}(x)\Gamma_n(t). \tag{A8}$$

Considering the homogeneous problem first, $\Phi_{in}(x)$ must satisfy,

$$\alpha_i \frac{\partial^2 \Phi_{in}}{\partial x^2} + \beta_{in}^2 \Phi_{in} = 0. \tag{A9}$$

which has the following solution,

$$\Phi_{1n} = C_{1n}\cos\left(\beta_{1n}x\right) + D_{1n}\sin\left(\beta_{1n}x\right), \tag{A10}$$

$$\Phi_{2n} = C_{2n}\cos\left(\beta_{2n}x\right) + D_{2n}\sin\left(\beta_{2n}x\right). \tag{A11}$$

The eigenvalues β_{2n} and β_{1n} may be related through the requirement that the time decay of the temperature at the interface $x = a$ must be identical for T_1 and T_2. This can only be true if

$$\alpha_1\beta_{1n}^2 = \alpha_2\beta_{2n}^2. \tag{A12}$$

Making the following definition

$$\gamma = \sqrt{\frac{\alpha_1}{\alpha_2}}, \quad \text{so that } \beta_{2n} = \gamma\beta_{1n}, \tag{A13}$$

and noting that one of the coefficients may be chosen arbitrarily, say $C_{1n} = 1$, the boundary conditions (A3–A5) may be applied to solve for the remaining coefficients D_{1n}, C_{2n}, and D_{2n}, with the consequent result,

$$\Phi_{1n} = \cos\left(\beta_{1n}x\right), \tag{A14}$$

$$\Phi_{2n} = \frac{-\delta\sin\left(\beta_{1n}x\right)\cos\left(\beta_{2n}(L-x)\right)}{\sin\left(\beta_{2n}(L-a)\right)}, \tag{A15}$$

where

$$\delta = \frac{k_1}{k_2}\gamma^{-1}.$$

The remaining interface condition, Eq. (A6), is used to derive the following transcendental equation for the eigenvalues

23

$$\Psi \beta_{1n} = \frac{1}{\tan{(\beta_{1n}a)}} + \frac{\delta}{\tan{(\beta_{1n}\gamma(L-a))}}, \tag{A16}$$

where

$$\Psi = \frac{k_1}{h}.$$

By assuming perfect thermal contact at the interface between the slabs, the resistance Ψ vanishes and Eq. (A16) then simplifies to,

$$\delta \tan{(\beta_{1n}a)} + \tan{(\beta_{1n}\gamma(L-a))} = 0. \tag{A17}$$

The roots are trivially found by employing a Newton-Raphson method within intervals bounded by the singular points,

$$\beta_{1n} = \frac{n\pi}{2(L-a)\gamma} \quad \text{and} \quad \frac{n\pi}{2a} \quad \text{for} \quad n = 1, 2, 3\ldots\ldots\infty. \tag{A18}$$

In order to satisfy the inhomogeneous problem, one can show that $\Gamma_n(t)$ needs to satisfy,

$$\frac{\partial \Gamma_n}{\partial t} + \beta_n^2 \Gamma_n = Q_n^*(x,t). \tag{A19}$$

Orthogonality of the eigenfunctions yields the following expansion,

$$Q_n^*(t) = \frac{\displaystyle\sum_{i=1}^{2} \int_{x_i}^{x_{i+1}} Q_i(x,t)\Phi_{in}(x)\,dx}{N}, \tag{A20}$$

with the norm,

$$N = \sum_{i=1}^{2} \frac{\alpha_i}{k_i} \int_{x_i}^{x_{i+1}} \Phi_{in}^2(x)\,dx. \tag{A21}$$

Given the initial conditions Eq. (A7) we can write a solution for Eq. (A19) as follows,

$$\Gamma_n(t) = e^{-\beta_n^2 t} \int_{t'=0}^{t} Q_n^*(t')\, e^{\beta_n^2 t'}\,dt'. \tag{A22}$$

Substituting this in Eq. (A8) yields,

$$T_i = \sum_{n=1}^{\infty} \Phi_{in}\, e^{-\beta_n^2 t} \int_{t'=0}^{t'=t} Q_n^*(t')\, e^{\beta_n^2 t'}\,dt'. \tag{A23}$$

24

The heat source in the present study consists of a surface heat flux of intensity $\bar{Q}(t)$ imposed on the surface $x = 0$. Making the substitution $Q_1(x,t) = \bar{Q}(t).\delta(x = 0)$ and $Q_2(x,t) = 0$ in Eq. (A20) and performing the necessary integrations gives,

$$Q_n^*(t) = \frac{\bar{Q}(t)}{N},$$

(A24)

where, from Eq. (A21),

$$N = \frac{2\beta_{1n}a + \sin 2\beta_{1n}x}{4\beta_{1n}} + \frac{\delta^2 \sin^2 \beta_{1n}a \ (2\gamma\beta_{1n}(L-a) + \sin 2\gamma\beta_{1n}(L-a))}{4\gamma\beta_{1n} \sin^2 \gamma\beta_{1n}(L-a)}.$$

(A25)

For a flux of fixed intensity, $\bar{Q}(t) = \bar{Q}$, the complete transient solution is,

$$T_1(x,t) = \sum_{n=1}^{\infty} \frac{\frac{\bar{Q}}{\alpha_1\beta_{1n}^2} \left(1 - e^{-\alpha_1\beta_{1n}^2 t}\right) \cos\beta_{1n}x}{N},$$

(A26)

and

$$T_2(x,t) = \sum_{n=1}^{\infty} \frac{1}{N} \frac{-\delta \sin(\beta_{1n}x) \cos(\beta_{2n}(L-x))}{\sin(\beta_{2n}(L-a))} \frac{\bar{Q}}{\alpha_1\beta_{1n}^2} \left(1 - e^{-\alpha_1\beta_{1n}^2 t}\right).$$

(A27)

At steady state, thermal equilibrium requires that,

$$T_1|_{t\to\infty} = T_2|_{t\to\infty} = \frac{\bar{Q}(\frac{k_1}{\alpha_1})a}{(\frac{k_1}{\alpha_1})a + (L-a)(\frac{k_2}{\alpha_2})}.$$

(A28)

The result is now appled to examine the effect of a paint layer on the structure depicted in Fig 21 when subjected to a constant heat flux of 2 millisecond duration. The substrate is a 10 mm thick aluminium plate with thermal conductivity and thermal diffusivity of 125 $Wm^{-1}K^{-1}$ and 49 $mm^2 sec^{-1}$ respectively and the corresponding paint properties are 0.2 $Wm^{-1}K^{-1}$ and 0.014 $mm^2 sec^{-1}$. The evolution of surface temperature is presented in Fig 22 for paint layer thicknesses varying from 0 to 100 μm and also for the case where the structure comprises only of paint.

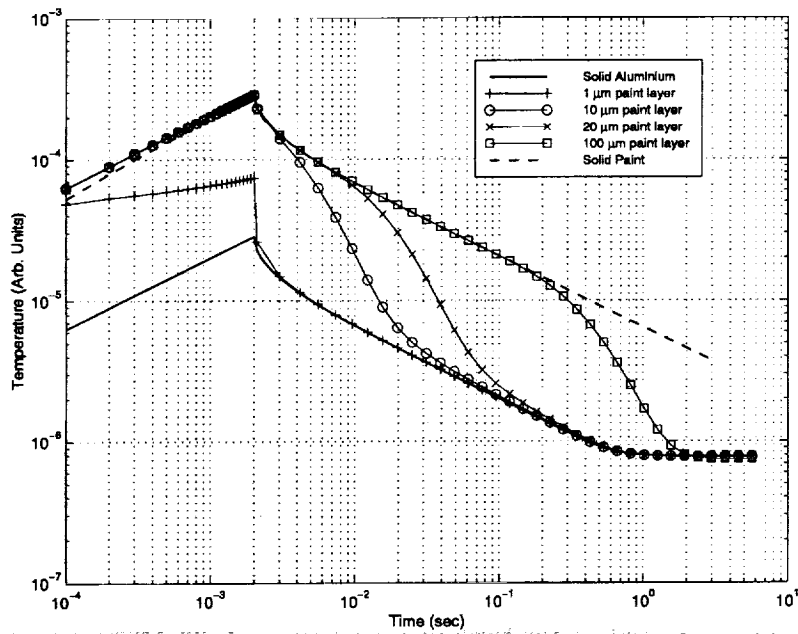Figure 22: Surface response ($x = 0$) as predicted by Eqns A26 and A28 for various paint layer thicknesses.

REPORT DOCUMENTATION PAGE		Form Approved OMB No. 0704-0188

1. AGENCY USE ONLY (Leave blank)	2. REPORT DATE June 1998	3. REPORT TYPE AND DATES COVERED Technical Publication

4. TITLE AND SUBTITLE
Quantitative Examination of Corrosion Damage by Means of Thermal Response Measurements

5. FUNDING NUMBERS
WU 538-02-11-01

6. AUTHOR(S)
Nik Rajic

7. PERFORMING ORGANIZATION NAME(S) AND ADDRESS(ES)

NASA Langley Research Center
Hampton, VA 23681-2199

8. PERFORMING ORGANIZATION REPORT NUMBER

L-17734

9. SPONSORING/MONITORING AGENCY NAME(S) AND ADDRESS(ES)

National Aeronautics and Space Administration
Washington, DC 20546-0001

10. SPONSORING/MONITORING AGENCY REPORT NUMBER

NASA/TP-1998-208429

11. SUPPLEMENTARY NOTES
Rajic: Visiting Scientist on a 1-year tenure from Aeronautical and Maritime Research Laboratory, Melbourne, Australia. Work performed at NASA Langley Research Center under the Aircraft Structural Integrity Program.

12a. DISTRIBUTION/AVAILABILITY STATEMENT
Unclassified-Unlimited
Subject Category 26   Distribution: Standard
Availability: NASA CASI (301) 621-0390

12b. DISTRIBUTION CODE

13. ABSTRACT (Maximum 200 words)
Two computational methods are presented that enable a characterization of corrosion damage to be performed from thermal response measurements derived from a standard flash thermographic inspection. The first is based upon a one dimensional analytical solution to the heat diffusion equation and presumes the lateral extent of damage is large compared to the residual structural thickness, such that lateral heat diffusion effects can be considered insignificant. The second proposed method, based on a finite element optimization scheme, addresses the more general case where these conditions are not met. Results from an experimental application are given to illustrate the precision, robustness and practical efficacy of both methods.

14. SUBJECT TERMS
Corrosion damage; Infrared thermography; Inverse heat conduction problem; Heat diffusion; Non-linear optimization; Finite element method; Least squares

15. NUMBER OF PAGES
31

16. PRICE CODE
A03

17. SECURITY CLASSIFICATION OF REPORT Unclassified	18. SECURITY CLASSIFICATION OF THIS PAGE Unclassified	19. SECURITY CLASSIFICATION OF ABSTRACT Unclassified	20. LIMITATION OF ABSTRACT